HHS Public Access

Author manuscript

Clin Neurophysiol. Author manuscript; available in PMC 2018 April 23.

Published in final edited form as:

Clin Neurophysiol. 2018 January ; 129(1): 296–307. doi:10.1016/j.clinph.2017.08.036.

Utilization of independent component analysis for accurate pathological ripple detection in intracranial EEG recordings recorded extra- and intra-operatively

Shoichi Shimamoto[a], **Zachary J. Waldman**[a], **Iren Orosz**[c], **Inkyung Song**[a], **Anatol Bragin**[d], **Itzhak Fried**[e], **Jerome Engel Jr.**[d], **Richard Staba**[d], **Ashwini Sharan**[b], **Chengyuan Wu**[b], **Michael R. Sperling**[a], and **Shennan A. Weiss**[a,*]

[a]Department of Neurology, Jefferson Comprehensive Epilepsy Center, Thomas Jefferson University, Philadelphia, PA, USA

[b]Department of Neurosurgery, Jefferson Comprehensive Epilepsy Center, Thomas Jefferson University, Philadelphia, PA, USA

[c]Department of Radiology, David Geffen School of Medicine, University of California Los Angeles, Los Angeles, CA, USA

[d]Department of Neurology, David Geffen School of Medicine, University of California Los Angeles, Los Angeles, CA, USA

[e]Department of Neurosurgery, David Geffen School of Medicine, University of California Los Angeles, Los Angeles, CA, USA

Abstract

Objective—To develop and validate a detector that identifies ripple (80–200 Hz) events in intracranial EEG (iEEG) recordings in a referential montage and utilizes independent component analysis (ICA) to eliminate or reduce high-frequency artifact contamination. Also, investigate the correspondence of detected ripples and the seizure onset zone (SOZ).

Methods—iEEG recordings from 16 patients were first band-pass filtered (80–600 Hz) and Infomax ICA was next applied to derive the first independent component (IC1). IC1 was subsequently pruned, and an artifact index was derived to reduce the identification of high-frequency events introduced by the reference electrode signal. A Hilbert detector identified ripple events in the processed iEEG recordings using amplitude and duration criteria. The identified ripple events were further classified and characterized as true or false ripple on spikes, or ripples on oscillations by utilizing a topographical analysis to their time-frequency plot, and confirmed by visual inspection.

Results—The signal to noise ratio was improved by pruning IC1. The precision of the detector for ripple events was 91.27 ± 4.3%, and the sensitivity of the detector was 79.4 ± 3.0% (N = 16

*Corresponding author at: Thomas Jefferson University, Department of Neurology and Neuroscience, Comprehensive Epilepsy Center, Computational Epilepsy Research Laboratory, 901 Walnut St., Suite 400, Philadelphia, PA 19107, USA. Fax: +1 215 503 3804. Shennan.Weiss@jefferson.edu (S.A. Weiss).

Conflict of interest statement

The author(s) declare(s) that there is no conflict of interest regarding the publication of this article.

patients, 5842 ripple events). The sensitivity and precision of the detector was equivalent in iEEG recordings obtained during sleep or intra-operatively. Across all the patients, true ripple on spike rates and also the rates of false ripple on spikes, that were generated due to filter ringing, classified the seizure onset zone (SOZ) with an area under the receiver operating curve (AUROC) of >76%. The magnitude and spectral content of true ripple on spikes generated in the SOZ was distinct as compared with the ripples generated in the NSOZ ($p < .001$).

Conclusions—Utilizing ICA to analyze iEEG recordings in referential montage provides many benefits to the study of high-frequency oscillations. The ripple rates and properties defined using this approach may accurately delineate the seizure onset zone.

Significance—Strategies to improve the spatial resolution of intracranial EEG and reduce artifact can help improve the clinical utility of HFO biomarkers.

Keywords

High-frequency oscillation; Ripple; Independent component analysis; Detector

1. Introduction

Approximately 30% of patients with epilepsy continue to have disabling seizures despite treatment with multiple antiepileptic drugs (Kwan and Brodie, 2000). Of those patients with focal epilepsy that are resistant to multiple medications, resective surgery is an intervention that has been proven to reduce the seizure burden, improve the patients' quality of life, and reduce mortality rate (Wiebe et al., 2001; Sperling et al., 2016). The goal of resective epilepsy surgery is to identify and remove epileptogenic brain regions while minimizing residual neurological deficits. High frequency oscillations (HFOs), which consist of brief bursts of energy with spectral content ranging between 80 and 600 Hz, have shown significant promise as a potential biomarker of epileptogenic tissue (Engel et al., 2009; Gotman, 2010; Jacobs et al., 2012). HFOs with a spectral content in the 80–250 Hz band are commonly referred to as ripples, while those in the 250–600 Hz band are termed fast ripples (Staba et al., 2002; Bragin et al., 2002).

HFOs can be identified by visual inspection of intracranial EEG (iEEG), or using automated and unsupervised detection software (Zelmann et al., 2012; Burnos et al., 2014; Gliske et al., 2016). One barrier to utilizing HFOs for clinical decision making is that inter-reader agreement on what constitutes an event is often poor (Spring et al., 2017). Therefore, it is difficult to validate automated HFO detectors. Furthermore, HFO detectors may generate clinically informative results (Weiss et al., 2013, 2015), in the absence of a gold standard comparison biomarker that can be confirmed visually. This paradox can perhaps be solved by developing a procedure to allow experts to code HFOs from iEEG signals using classes (Jacobs et al., 2008) that generate an agreed upon gold standard for evaluating automated procedures.

HFO detection is performed using recordings in bipolar montage in order to reduce artifact, originating from muscle or the reference electrode, that can mimic HFO events. There are no previously published studies that utilize an automated HFO detector to define events in

macroelectrode recordings recorded in referential montage. In theory, performing HFO detection in referential montage provides two advantages. First, referential montage increases the spatial resolution of the iEEG as compared with bipolar montage by increasing the total number of recordings. Second, referential montage could improve HFO detection by increasing the signal to noise ratio, since the dipole generators of the HFO could be distributed across multiple macro-electrode sites, which could obscure the HFO due to in phase cancellation (de la Prida et al., 2016).

In order to identify HFOs in referential montage using an automated detector, it is essential to develop a strategy for reducing or eliminating artifact, that would otherwise be eliminated by a bipolar montage. Independent component analysis (ICA) is a signal processing approach that can separate signal sources based on minimizing mutual information, and assuring that each component has a non-Gaussian distribution (Bell and Sejnowski, 1995; Cardoso, 1997). ICA has been utilized to reduce artifact in scalp EEG (Delorme et al., 2007; McMenamin et al., 2010), and has also been used to remove the scalp reference signal from iEEG recordings (Hu et al., 2007). In this paper, we tested the hypothesis that applying ICA to band-pass filtered iEEG recordings in referential montage could be utilized to accurately detect ripple events even when the recordings are contaminated by artifact.

2. Methods

2.1. Patients

Recordings were selected from 11 patients who underwent intracranial monitoring with depth electrodes between 2014 and 2016 at University of California Los Angeles (UCLA) and from five patients at Thomas Jefferson University (TJU) in 2016–2017 for the purpose of localization of the seizure onset zone. The inclusion criteria were at least one night and day of intracranial recording with 2000 Hz sampling rate and at least 4 h of interictal EEG uninterrupted by seizures for the UCLA patients. For the TJU patients inclusion criteria were at least 10 min of intra-operative recordings from acutely implanted depth electrodes. The TJU intra-operative recordings were performed when the patient was anesthetized with 2% sevoflurane and 0.08 mcg/kg/min of remifentanil.

All clinical data from the patient’s inpatient and postsurgical follow-up charts were available for review. Patients underwent pre-surgical magnetic resonance imaging (MRI) and stereotactic electrode implantation, as well as a CT scan to localize electrodes after implantation and a postsurgical MRI after the respective surgery. All patients provided verbal and written consent prior to participating in this research which was approved by the UCLA and TJU institutional review boards.

Seizure onset zone (SOZ) was defined as the brain tissue that contained the intracranial electrode that captured the onset of seizures. SOZ was determined by visual inspection of iEEG recordings as a part of the routine clinical evaluation for resective surgery in a bipolar montage. If the ictal onset was not evident in both electrode pairs, that electrode was not considered part of the SOZ.

2.2. EEG recordings and segment selection

Clinical iEEG (0.1–600 Hz; 2000 samples per second) was recorded from 7 to 15 contact depth electrodes using a Nihon-Kohden 256-channel JE-120 long-term monitoring system (Nihon-Kohden America, Foothill Ranch, CA, U.S.A.) for the sleep recordings, and at (0.1–400 Hz; 1000 samples per second) for two of the intra-operative recordings. The sleep recordings were confirmed by video-EEG inspection revealing K-complexes, spindles, slow waves, and a paucity of muscle artifact. We did not perform concurrent electrooculography (EOG) and electromyography (EMG) recordings. The reference signal used for the recordings performed at UCLA was a scalp Fz electrode. The reference signal used for the TJU intra-operative recordings was a bipolar subtraction of electrodes #5 and #6 which is the default setting for Nihon Kohden JE-120 amplifiers. The 8 min segments of sleep recordings used in this study were selected on the basis of overall recording quality as determined by visual inspection by a board certified neurologist with fellowship training in epilepsy (SW) using BESA v5 (Gräfelfing, Germany).

2.2.1. Data processing—All iEEG data was imported from EDF format into Matlab v2016b (Natick, MA). Subsequent processing steps were all performed using custom software developed in Matlab. Only iEEG recordings from channels deemed suitable on the basis of visual inspection (SW) were analyzed by the automated and unsupervised detector.

2.2.2. Artifact reduction for ripple detection from referential montage EEG recordings—Each iEEG recording was band-pass filtered using a 500th order digital symmetric finite impulse response (FIR) filter between (80–600 Hz) for the sleep recordings sampled at 2 kHz, and (80–400 Hz) for the intra-operative recordings sampled at 1 kHz. Infomax independent component analysis (Lee et al., 1999) was applied to the entire band pass (80–600 Hz) or (80–400 Hz) filtered referential montage recordings using the CUDAICA implementation (Raimondo et al., 2012), the number of independent components was equal to the number of recording electrodes. The first independent component was pruned, and an artifact index AI(t) was calculated to exclude artefactual events;

$$AI(t) = \frac{\mid hfo_i(t) - ic1_i(t) \mid}{\sum \mid hfo_i(t) \mid / T} * \frac{1}{I} \sum_i^I \frac{\mid hfo_i(t) - ic1_i(t) \mid}{\sum \mid hfo_i(t) \mid / T} \quad (1)$$

where $hfo_i(t)$ is the band pass filtered EEG or LFP recording (i), and $ic1_i(t)$ is the band pass filtered EEG or LFP recording (i) after pruning the first independent component.

2.2.3. Ripple event detection—Ripples were detected by applying a Hilbert transform to calculate the instantaneous amplitude of this time series according to the analytic signal z(t) of $ic1_i(t)$ as described in Eq. (2).

$$z(t) = a(t)e^{i\phi(t)} \quad (2)$$

where a(t) is the instantaneous amplitude and phi(t) is the instantaneous phase of z(t). For bipolar recordings the analytic signal z(t) was calculated from the band-pass (80–600 Hz) or (80–400 Hz) filtered iEEG time series.

The instantaneous HFO amplitude function was smoothed using moving window averaging, and then the smoothed instantaneous HFO amplitude function was normalized using the mean and standard deviation of the time series. Smoothing increased the reliability of detection using the amplitude envelope, because of erratic cycle to cycle variability.

The onset of a potential discrete HFO event in the raw time series was triggered as the time point at which the smoothed and normalized HFO amplitude function exceeded a value of 3.5 standard deviations, the offset of the discrete HFO events was defined as the time point at which the smoothed and normalized HFO function fell below 1.5 standard deviations.

For each detected candidate event, we used a power spectral density function using the FFT spectra to calculate the peak frequency. A minimum duration criterion was applied to each detected event with a threshold based on its mean frequency; events that did not meet the criterion of an HFO, at least 3–4 cycles (approx. duration 25 ms) were excluded (Jacobs et al., 2008). For referential recordings, increases in high frequency (>80 Hz) amplitude occurring during epochs contaminated by artifact were identified on the basis of $AI(t)$ exceeding a value of 10, and were excluded. The duration of the events defined using this method was not the actual duration of the event, but only used for the purpose of defining event epochs.

HFOs were detected across all the intracranial macroelectrodes in twenty second bins, and only ripple events with a peak spectral content between (80–150 Hz) were subjected to further analysis. Each of these ripple events was stored as a one second trial of unfiltered iEEG.

Further processing of the extracted and exported ripple events in 1 s iEEG trials (see 2.3.5) were used to define the frequency-weighted power, mean frequency, and duration of the ripple events. This further processing was necessary, in part, because moving average filtering can affect the estimation of the duration.

2.2.4. Visual validation of ripple events—To assess the performance of the automated ripple detection algorithm, a gold standard for ripples was established by visual inspection of 8 min bandpass filtered iEEG segments by two independent reviewers (SW, SS) in referential montage. The annotated EDF files generated by the ripple detector, prior to time-frequency analysis (see 2.3.5), were reviewed using the following settings: 2 s per page with a high-pass zero phase filter with a cutoff at 80 Hz, slope of 48 dB/oct, and a low-pass zero phase filter with a cut off at 200 Hz, and slope of 48 dB/oct. The purpose of the validation was to determine whether the demarcation of the ripple events was sensitive and precise. No information regarding the ripple type, duration, frequency, or power was provided. For the visual inspection, a ripple was defined as brief (3–4 cycles) high frequency oscillations (80–200 Hz) with amplitude that exceeded two-three times that of the background amplitude. Events that were annotated by the automated algorithm were visually inspected as true

positive or false positive, while the iEEG was also visually inspected for false negative events. We used the following definitions; true positive (TP): a ripple annotated by the detector and confirmed on visual inspection, false positive (FP): a ripple annotated by the detector that was not confirmed on visual inspection, false negative (FN): a ripple confirmed on visual inspection that was not annotated by the detector, true negative (TN): an entire 8 min epoch containing no ripples on visual inspection, that also contained no ripple annotations. The sensitivity was defined as TP/(TP + FN), the precision as TP/(TP + FP). We could not define the specificity, or NPV because the TN definition was not equivalent to the other metrics due to recording duration.

2.2.5. Differentiation of true ripple on spike events from false ripple on spike events resulting from filter ringing and quantification of ripple properties—The one second iEEG trials containing ripple events as determined by the detection algorithm underwent further processing by a custom automated algorithm that distinguished true from false ripple events using wavelet convolution, identifying contours of isopower, and then categorizing these contours into sets of open or closed loop groups (Waldman et al., 2018). This custom algorithm has been previously validated using simulated data and by visual inspection of iEEG data. The results are pending review for publication at this time. The events with closed loops were considered to be true ripple events, whereas those with open loops were thought to be false ripples due to artifact from applying a bandpass filter to sharp transient waveforms. The theoretical background for this algorithm is that time-frequency analysis of true ripple events produce “blobs” of power within the ripple frequency range (80–200 Hz) (Bénar et al., 2010). In contrast, sharply contoured epileptiform discharges that result in ripple-band activity following band-pass filtering produce “candles” of power. If the isopower contours of the respective time-frequency plots for these two types of events are characterized, the true ripple events exhibit closed loop groups, while the false ripple on spike events produce open loop contours because the “candle” of power extends below the ripple band. Four properties were extracted from the closed-loop contour event region in the case of true oscillations. The first two were times of event onset and offset for determination of the event duration. These onset and offset times were defined as the minimum and maximum time coordinates associated with the vertices of the boundary contour. To determine the magnitude of each true ripple the algorithm summated across all coordinate points of the time-frequency map within the boundary B, of the event. The amplitude-weighted mean frequency of the HFO event was calculated using:

$$\overline{f_{hfo}} = \sum_{i}^{B} \frac{f_i * P_i}{\sum P_i} \quad (3)$$

where f_i and P_i and are the frequency and power amplitude of coordinate of the TF map within the boundary contour, B.

Simulations were used to measure the stability and reliability of the measurements of ripple properties on the basis of the topographical analysis (Waldman et al., 2018).

2.2.6. Differentiation of true ripple on spike events from ripple on oscillations—To distinguish true ripples that occur during epileptiform spikes from all other ripples, we calculated the derivative of the peri-ripple band-pass filtered (4–30 Hz) iEEG and applied a threshold of 4 μV/msec. The one second iEEG trials containing ripple events that exceeded this threshold within ±50 ms of the peak amplitude of the ripple were inspected and categorized as ripples on spikes. All other true ripples were categorized as ripples on oscillations. The results of the automated algorithm were validated by visual inspection (SW). For visual confirmation, a ripple on spike was defined as any true ripple that was superimposed on an epileptiform spike, which was visually detected on raw iEEG.

2.2.7. Statistical analysis—The SOZ rate ratio for ripple events was calculated using

$$rr_{soz} = \left(\frac{Mean\ Event\ Rate_{SOZ} - Mean\ Event\ Rate_{NSOZ}}{Mean\ Event\ Rate_{SOZ} + Mean\ Event\ Rate_{NSOZ}} \right) \quad (4)$$

Paired and unpaired student's *t*-test were two tailed with a 0.05 significance level. Receiver operating characteristic curves (Peacock, 1983) and the two-dimensional Kolmogorov-Smirnov test (Davis and Goadrich, 2006) were implemented in Matlab.

3. Results

3.1. Patient description

The recordings were selected from eleven patients who underwent intracranial monitoring with depth electrodes during sleep, and five patients in which the intracranial monitoring was performed in the operating room using depth electrodes. Among the patients in whom the sleep recordings were selected, three had unilateral mesial temporal lobe epilepsy (MTLE), three patients had bilateral MTLE, three patients had MTLE plus the involvement of neocortical regions, and two patients had neocortical epilepsy (Table 1). Among the patients in whom the intra-operative recordings were selected, two had unilateral MTLE, one had bilateral MTLE, and two had neocortical epilepsy.

3.2. Data analysis pipeline

Raw iEEG data in referential montage were visually inspected. Each recording was eight minutes in duration. Recordings from electrodes with poor signal quality were excluded from further analysis. Typically, the number of excluded electrodes was less than 10% of the total number of electrodes. The raw referential montage iEEG data underwent analysis by the automated and unsupervised process (Fig. 1), followed by visual validation of ripple events in the annotated iEEG files. Overall, in the referential montage recordings, 16,139 ripple events were detected in 790 macroelectrode contacts by the automated detector. As a control experiment, the recordings were also analyzed by the Hilbert HFO detector in bipolar montage. In this case, 15,350 ripple events were detected in 711 macroelectrode contacts.

3.3. Utility of independent component analysis for muscle artifact reduction and ripple detection

Artifact often mimicked HFOs in band-pass filtered referential recordings (Fig. 2B). Among the 16 iEEG recordings from the individual patients, 15 were contaminated with at least one epoch of artifact evident to varying degrees simultaneously across all the recording electrodes. When these iEEG recordings were processed with Infomax ICA after band-pass filtering (80–600 Hz) the artifact could be reduced or removed by pruning the first independent component (IC1) (Fig. 2C). We visually inspected the individual ICs, across all the iEEG electrode recordings, to determine whether all the muscle artifact was isolated to IC1 alone. We found that IC1 often contained most of the artefactual signal, but other ICs also contained artefactual signals of a lesser magnitude (Supplementary Fig. S1). Notably, signals containing HFOs across were often isolated to individual components (Supplementary Fig. S2). An artifact index derived from IC1 could be used to reject artefactual events in the cases when the artifact was not removed entirely after pruning IC1 (Fig. 2C). Pruning IC1 also resulted in a reduction in the baseline signal amplitude and enhanced the signal to noise ratio, since the mean absolute signal amplitude was reduced from 1.56 ± 0.03 uV to 1.23 ± 0.02 uV ($n = 624$, $p = 0$, paired t-test). For some ripple events, pruning IC1 also improved the morphology leading to more accurate detection (Fig. 2C). One pitfall of the ICA method was that in one patient (UC_456) HFOs were incorrectly removed along with the artifact in several electrodes when IC1 was pruned (Table 2).

3.4. Validation of the ICA ripple detector by visual inspection

We validated the annotations from the ripple detector in a subset of ten referential montage channel recordings for each of the 16 patients using visual review of the unfiltered and band-pass filtered iEEG. Each of the computer generated annotations was classified as a true or false positive, and additional annotations were added by the reviewer for false negative HFO detections, irrespective of the HFO type. Overall, over 5842 annotations were used to assess the performance of the detector. The precision of the detector for ripple events was 91.27 ± 4.3% (Table 2), and the sensitivity of the detector was 79.4 ± 3.0% ($N = 160$, $n = 160$ electrodes). Our validation methodology could not directly assess the true negative cases, however, among the ten distinct iEEG recordings inspected per patient, an average of 33.0 ± 6.0% ($n = 16$) exhibited zero false negative HFO detections. Detector performance was variable across patients, for instance the sensitivity of patient 456 was near chance at 53.14%, and the sensitivity of TJU_006 was only 64.0%, in contrast the sensitivity of TJU_004 was 95.5%.

The inter-reader agreement among two readers (SW, SS) for detector validation was Cohen's kappa = 0.52 ± 0.09 (observed agreement 82.75 ± 4.11%, $p < 1e–4$, $N = 13$, $n = 2264$ ripple events). The sensitivity and precision of ripple detection was similar in recordings obtained during sleep and in the operating room (unpaired t-test, $n = 11,5$, $p = .71$ for sensitivity, $p = .06$ for precision).

3.5. Distinguishing true from false ripple events

Of the 16,139 ripple events detected in the referential montage recordings, 5989 (33.0%) were found to be true ripple oscillations while the remaining events were generated as a

result of filter ringing. Of the 15,350 ripple events detected in the bipolar montage recordings, 8759 (49.6%) were found to be true ripple events. The validity and accuracy of this second stage of detection is detailed in Waldman et al., 2018.

To clarify, the iEEG ICA ripple detector detailed in Section 3.4 extracted iEEG trials with ripple events for subsequent analysis irrespective of whether the ripples were true oscillations or resulted from filtering sharp epileptiform discharges. Consequently, the sensitivity and precision of the detector provided in Section 3.4 refers to the combined detection of both types of events.

3.6. Distinguishing true ripple on spikes from true ripple on oscillations

To determine whether true ripples occurred on spikes or oscillations, we applied an automated and unsupervised process (Fig. 3, see methods). Based on visual validation by a single observer, the sensitivity of this process was 92.1 ± 3.0%, specificity of this process was 68.8 ± 6.5%, precision (i.e. PPV) was 70.9 ± 6.1%, and NPV 81.9 ± 2.4% (n = 2300 ripple events, N = 12 patients). Of the 5989 true ripple events detected in the referential montage recordings, 2305 (38.5%) were determined to be ripples on spikes, and the others ripples on oscillations.

3.7. Accuracy of the detected ripples for the seizure onset zone

We next addressed whether or not the rates of the different ripple types quantified by the detector could be used to distinguish the SOZ. For all 16 patients, including the five patients with iEEG recordings performed intra-operatively, the mean ripple rates of true and false ripples on spikes recorded inside the SOZ was almost always greater as compared with the non-SOZ (NSOZ), however this was less often the case for ripples on oscillations (Fig. 4). Notably, true and false ripples on spikes were similar with respect to the SOZ rate ratio that compares the mean ripple rate in the SOZ with the mean ripple rate in the NSOZ (n = 16, p = .21, paired t-test, Fig. 4). In contrast, The SOZ rate ratio for ripples on oscillations was decreased with respect to the true ripples on spikes (n = 16, p < .01, paired t-test, Fig. 4A). These differences between the ripple types were also evident in the recordings analyzed in bipolar montage (Supplementary Fig. S3). Overall, the SOZ rate ratios derived from the recordings in referential montage were slightly increased as compared with the SOZ rate ratios derived from the bipolar montage recordings. This difference met statistical significance for the false ripple on spike SOZ rate ratio (paired t-test, n = 16 p < .05). We also generated receiver operating characteristic (ROC) curves for classifying the seizure onset zone on the basis of unscaled ripple rate measurements across all patients in either the sleep, or intra-operative patient cohorts (Fig. 5). Unfortunately, the sample size was too small to address statistical significance of changes in the montage using the ROC methodology. Overall, the classification accuracy of true and false ripple on spike rates for the seizure onset zone was good and the area under the ROC (AUROC) was >76%.

3.8. Differences in the spectral content and power of ripples inside and outside the SOZ

We next asked if the properties of ripples, such as spectral content or power, differed depending on whether the event was generated in the SOZ or NSOZ. For true ripples on spikes measured using referential montage it appeared that the events recorded from the

NSOZ were of a lower spectral content and lower power as compared with the events recorded from the SOZ. A two-dimensional Kolmogorov-Smirnov test confirmed that the populations or ripple events in the SOZ and NSOZ were distinct when classified by spectral content and power (KS = 0.239, p = 7.6e–11, Fig. 6). A similar difference was also seen for the events measured during the intra-operative referential montage recordings (KS = 0.362, p = 3.8e–13, Fig. 6). In contrast, the properties of ripples on oscillations did not strongly depend on whether they were generated in the SOZ or NSOZ (KS = 0.167, p = 4.3e–5, Fig. 6). The use of bipolar montage recordings reduced the differences between the properties of true ripple on spike events generated in the SOZ as compared with the NSOZ (KS = 0.174, p = .1.3e–5, Supplementary Fig. S4).

4. Discussion

In summary, herein we report that (1) by processing band-pass filtered (80–600 Hz) iEEG signals recorded in referential montage with Infomax ICA we could reduce or eliminate muscle artifact, and demarcate artefactual HFOs, (2) manual validation demonstrated that when a Hilbert detector was used to detect the ripple events in the post-ICA processed referential recordings, it was moderately sensitive and very precise, (3) both the true and false ripple on spike events defined using the detector were equally accurate for identifying the SOZ, but the ripples on oscillations less so, (4) true ripple on spikes generated in the seizure onset zone (SOZ) were distinct with respect to spectral content and power as compared to the NSOZ.

4.1. Advantages and pitfalls of utilizing independent component analysis prior to ripple detection

It has been proposed that the scalp reference signal can be isolated in iEEG recordings using ICA (Hu et al., 2007). Our results are compatible with this conclusion. When Infomax ICA is applied the derived first independent component (i.e. IC1) is the signal that explains the maximal variance across all the recording electrodes (Bell and Sejnowski, 1995; Lee et al., 1999). In band-pass filtered recordings in referential montage most of the variance across all the recording electrodes is accounted for by muscle artifact in the reference signal. Therefore, by pruning IC1 the artifact in the reference signal is removed or reduced from the band-pass filtered iEEG recordings. When residual reference signal remains, the artifact index can be utilized to reject the artefactual HFOs on the basis of the relative differences between the original and the pruned signals across electrodes.

One pitfall of using ICA to remove the reference signal from iEEG signals is that HFOs can also be removed when IC1 is pruned. The mixing matrix for IC1 may be weighted heavily in recordings from signals with elevated HFO rates. In this study, we found that “HFO stripping” only occurred in several electrodes recorded from one of the 16 patients. It would be feasible to prevent HFO stripping by utilizing an automated algorithm to define the recordings in which it occurs, and selectively not pruning IC1 in those recordings. While this would increase the sensitivity of HFO detection, it would also potentially decrease the precision because of residual artifact that may be detected as ripples by the Hilbert detector. A second pitfall of this approach is that the threshold for excluding artefactual HFOs based

on the artifact index is arbitrary. Pathophysiological HFOs could be rejected, thereby reducing sensitivity of the detector.

Another method to improve the accuracy of HFO detection utilizing ICA is to first determine which ICs contain the HFO signals and then to isolate these signals by pruning all other components. The signal to noise ratio would then be vastly increased and even relatively small amplitude events could be detected using a low cut-off threshold.

4.2. Accuracy of ripple detection following independent component analysis

The Hilbert detector utilized amplitude and duration threshold criteria to detect ripple events in the band-pass filtered iEEG following the pruning of IC1. Visual validation confirmed that the Hilbert detector had excellent precision even in iEEG recordings contaminated with muscle. Unfortunately, our estimate of the detectors sensitivity and precision was likely inflated because the external golden reference, in this case visual inspection of the iEEG, depended on the experimental procedure because the iEEG records had been annotated by the software. One reason our detector exhibited excellent precision, even with confounding artifact, is that pruning IC1 improved the signal to noise ratio of ripples over the baseline of the signal, and improved the morphology of pathophysiological ripples.

Unfortunately, our detector was only moderately sensitive, and across all the patients all the events were rarely detected. While the sensitivity of our detector could be improved by decreasing the amplitude threshold for event detection, the utilization of ICA introduced confounds that impacted detector sensitivity such as HFO stripping, and the rejection of pathophysiological events due to lower than optimal artifact index threshold. The cost of these confounds may be outweighed by the improved spatial resolution of our detector.

4.3. Delineation of the seizure onset zone using ripple rates defined by the detector

The ripple events defined by the detector occurred primarily in the SOZ. A 2–5-fold increase in the rate of ripples in the seizure onset zone, relative to the NSOZ, was evident in patients with mesial temporal lobe epilepsy, mesial temporal lobe epilepsy plus (Barba et al., 2007, 2016), and neocortical epilepsy. The accuracy of ripple rates for classifying the SOZ is consistent with previously published studies (Jacobs et al., 2008, 2009; Worrell et al., 2008; Wang et al., 2013; Weiss et al., 2016).

In intraoperative iEEG recordings from depth electrodes, ripple rates were also dramatically increased in the SOZ. Therefore, ripples recorded under anesthesia from standard SEEG macroelectrodes can potentially delineate the SOZ, despite the confound of injury potentials (Ulbert et al., 2004). The finding also provides proof of principle that this detector can effectively reduce the artifacts that occur in the intra-operative setting.

In both the sleep and intra-operative recordings the accuracy of true and false ripple on spikes were superior to ripples on oscillations. Prior investigations have also demonstrated that ripples on spike rates are better than ripple on oscillation rates for delineating the seizure onset zone (Wang et al., 2013; Weiss et al., 2016).

The equivalent utility of true and false ripple on spikes for delineating the SOZ should not be interpreted as evidence that ripples and inter-ictal discharges are eqully useful for identifying epileptogenic regions. False ripples on spikes are not synonymous to all inter-ictal discharges without a ripple. For epileptiform discharges, waveform shape (Cole and Voytek, 2016) may be a critical factor. False ripples on spikes are generated by very sharply contoured epileptiform discharges that may be generated by a distinct mechanism such as a synchronized burst of action potentials *i.e.* population spikes (Zhang et al., 2014).

4.4. Differences between true and false ripple on spikes

In this study we used a new topographic method (Waldman et al., 2018) to separate true ripple on spikes from false ripple on spikes that result from filtering inter-ictal discharges (Bénar et al., 2010). In accord with other published literature (Burnos et al., 2016), both true and false ripples on spike rates were equivalently increased in the SOZ as compared with the NSOZ.

Nonetheless, differentiating between true and false ripples on spikes was advantageous. In the case of a false ripple on spike, a ripple is not actually superimposed on the discharge, thus a measurement of the spectral content and power of the oscillation generated by band-pass filtering the sharply contoured discharge lacks concrete meaning (Eissa et al., 2016; Smith et al., 2016). In contrast, for true ripple on spikes the spectral content and power of the ripple oscillation can be accurately measured. When we compared the spectral content and power of true ripple on spike events generated in the SOZ with the true ripple on spike events generated in the NSOZ, we observed a strong significant difference. Prior reports have also found that ripples generated in the SOZ have a larger amplitude and lower spectral content as compared with ripples generated in the NSOZ (Matsumoto et al., 2013). Our results suggest that new approaches for defining epileptogenic regions could potentially be derived that utilize both the rate of different HFO types, as well as HFO properties such as magnitude and spectral content.

4.5. Differences in delineating the SOZ using bipolar vs. referential montage recordings

We found that, for the true ripple on spike events, the properties (*i.e.* spectral content and power) of the events generated in the SOZ, as compared with the NSOZ, became more distinct when referential montage recordings were used as opposed to bipolar montage recordings. It is possible that bipolar montage interferes with an accurate measurement of ripple spectral content and power when the generator dipole is distributed across neighboring recording contacts due to in phase cancellation.

5. Conclusions

We report a novel approach to identify and classify ripple events in iEEG recordings in the referential montage that eliminates or dramatically reduces artifact using Infomax ICA. The detector could also separate true ripple on spike events from false ripple on spike events that result from filter ringing, and accurately define the magnitude and spectral content of the true events. The true and false ripple on spike rates defined by the detector accurately classified the SOZ in a diverse group of patients with intracranial depth electrode implants

recorded during sleep or intra-operatively. In addition, the spectral content and power of true ripple on spike events generated in the SOZ were distinct from the events generated in the NSOZ. Future work will focus on improving the sensitivity of this detector, and also utilizing a similar approach to detect fast ripple events. ICA can likely be utilized to improve HFO detection in other types of iEEG data obtained from subdural electrode recordings for instance, and could also be used to detect HFOs in the local field potential recorded from microelectrodes. It may also be possible to apply ICA to scalp recordings (Weiss et al., 2017) to improve the detection of HFOs.

Supplementary Material

Refer to Web version on PubMed Central for supplementary material.

Acknowledgments

The authors would like to thank Mr. Dale Wyeth and Mr. Edmund Wyeth at Thomas Jefferson University, and Mr. Kirk Shattuck at University of California Los Angeles for their technical assistance with the experiments.

Funding

This work was supported by NIH/NINDS K23NS094633 (SAW).

References

Barba C, Barbati G, Minotti L, Hoffmann D, Kahane P. Ictal clinical and scalp-EEG findings differentiating temporal lobe epilepsies from temporal 'plus' epilepsies. Brain. 2007; 130:1957–67. [PubMed: 17535836]

Barba C, Rheims S, Minotti L, Guénot M, Hoffmann D, Chabardès S, et al. Temporal plus epilepsy is a major determinant of temporal lobe surgery failures. Brain. 2016; 139:444–51. https://doi.org/10.1093/brain/awv372. [PubMed: 26700686]

Bell AJ, Sejnowski TJ. Information-maximization approach to blind separation and blind deconvolution. Technology. 1995; 1159:1129–59. https://doi.org/10.1162/neco.1995.7.6.1129.

Bragin A, Mody I, Wilson CL, Engel J Jr. Local generation of fast ripples in epileptic brain. J Neurosci. 2002; 22:2012–21. [PubMed: 11880532]

Bénar CG, Chauvière L, Bartolomei F, Wendling F. Pitfalls of high-pass filtering for detecting epileptic oscillations: a technical note on "false" ripples. Clin Neurophysiol. 2010; 121:301–10. [PubMed: 19955019]

Burnos, S., Hilfiker, P., Sürücü, O., Scholkmann, F., Krayenbühl, N., Grunwald, T., et al. Human intracranial high frequency oscillations detected by automatic time-frequency analysis. PLoS ONE. 2014. https://doi.org/10.1371/journal.pone.0094381

Burnos S, Frauscher B, Zelmann R, Haegelen C, Sarnthein J, Gotman J. The morphology of high frequency oscillations does not improve delineating the epileptogenic zone. Clin Neurophysiol. 2016; 127:2140–8. https://doi.org/10.1016/j.clinph.2016.01.002. [PubMed: 26838666]

Cardoso J-F. Infomax and maximum likelihood for blind source separation. IEEE Signal Process Lett. 1997; 4(4):112–4. https://doi.org/10.1109/97.566704.

Cole SR, Voytek B. Brain oscillations and the importance of waveform shape. Trends Cognitive Sci. 2016; 21:137–49. https://doi.org/10.1016/j.tics.2016.12.008.

Davis, J., Goadrich, M. The relationship between precision-recall and ROC curves. ICML '06 proceedings of the 23rd international conference on machine learning; 2006; p. 233-40.doi: https://doi.org/10.1145/1143844.1143874

Delorme A, Sejnowski TJ, Makeig S. Enhanced detection of artifacts in EEG data using higher-order statistics and independent component analysis. Neuroimage. 2007; 34:1443–9. https://doi.org/10.1016/j.neuroimage.2006.11.004.9. [PubMed: 17188898]

Eissa, TL., Tryba, AK., Masrcuccilli, CJ., Ben-Mabrouk, F., Smith, EH., Lew, SM., et al. Multiscale aspects of generation of high-gamma activity during seizures in human neocortex; eNeuro. 2016. p. 3doi: https://doi.org/10.1523/ENEURO.0141-15.2016

Engel J, Bragin A, Staba R, Mody I. High-frequency oscillations: what is normal and what is not? Epilepsia. 2009; 50:598–604. https://doi.org/10.1111/j.1528-1167.2008.01917.x. [PubMed: 19055491]

Gliske SV, Irwin ZT, Davis KA, Sahaya K, Chestek C, Stacey WC. Universal automated high frequency oscillation detector for real-time, long term EEG. Clin Neurophysiol. 2016; 127:1057–66. https://doi.org/10.1016/j.clinph.2015.07.016. [PubMed: 26238856]

Gotman J. High frequency oscillations: the new EEG frontier? Epilepsia. 2010; 51(SUPPL 1):63–5. https://doi.org/10.1111/j.1528-1167.2009.02449.x. [PubMed: 20331719]

Hu S, Stead M, Worrell GA. Automatic identification and removal of scalp reference signal for intracranial eegs based on independent component analysis. IEEE Trans Biomed Eng. 2007; 54:1560–72. https://doi.org/10.1109/TBME.2007.892929. [PubMed: 17867348]

Jacobs J, LeVan P, Chander R, Hall J, Dubeau F, Gotman J. Interictal high-frequency oscillations (80–500 Hz) are an indicator of seizure onset areas independent of spikes in the human epileptic brain. Epilepsia. 2008 Nov.49:1893–907. https://doi.org/10.1111/j.1528-1167.2008.01656.x. [PubMed: 18479382]

Jacobs J, Zelmann R, Jirsch J, Chander R, Dubeau CÉCF, Gotman J. High frequency oscillations (80–500 Hz) in the preictal period in patients with focal seizures. Epilepsia. 2009; 50:1780–92. https://doi.org/10.1111/j.1528-1167.2009.02067.x. [PubMed: 19400871]

Jacobs J, Staba R, Asano E, Otsubo H, Wu JY, Zijlmans M, et al. High-frequency oscillations (HFOs) in clinical epilepsy. Prog Neurobiol. 2012; 98:302–15. https://doi.org/10.1016/j.pneurobio.2012.03.001. [PubMed: 22480752]

Kwan P, Brodie MJ. Early identification of refractory epilepsy. N Engl J Med. 2000; 342:314–9. [PubMed: 10660394]

Lee TW, Girolami M, Sejnowski TJ. Independent component analysis using an extended infomax algorithm for mixed subgaussian and supergaussian sources. Neural Comput. 1999; 11:417–41. [PubMed: 9950738]

Matsumoto A, Brinkmann BH, Matthew Stead S, Matsumoto J, Kucewicz MT, Marsh WR, et al. Pathological and physiological high-frequency oscillations in focal human epilepsy. J Neurophysiol. 2013; 110:1958–64. https://doi.org/10.1152/jn.00341.2013. [PubMed: 23926038]

McMenamin BW, Shackman AJ, Maxwell JS, Bachhuber DR, Koppenhaver AM, Greischar LL, et al. Validation of ICA-based myogenic artifact correction for scalp and source-localized EEG. Neuroimage. 2010; 49:2416–32. https://doi.org/10.1016/j.neuroimage.2009.10.010. [PubMed: 19833218]

Menendez de la Prida L, Staba RJ, Dian JA. Conundrums of high-frequency oscillations (80–800 Hz) in the epileptic brain. J Clin Neurophysiol. 2016; 8:583–92. https://doi.org/10.1002/aur.1474.Replication.

Peacock JA. Two-dimensional goodness-of-fit testing in astronomy. Monthly Notices Roy Astron Soc. 1983; 202:615–27.

Raimondo, F., Kamienkowski, JE., Sigman, M., Fernandez Slezak, D. CUDAICA: GPU optimization of infomax-ICA EEG analysis; Comput Intell Neurosci. 2012. p. 206972doi: https://doi.org/10.1155/2012/206972. Epub 2012 Jul 3

Staba RJ, Wilson CL, Bragin A, Fried I, Engel J. Quantitative analysis of high-frequency oscillations (80–500 Hz) recorded in human epileptic hippocampus and entorhinal cortex. J Neurophysiol. 2002; 88:1743–52. [PubMed: 12364503]

Smith EH, Liou JY, Davis TS, Merricks EM, Kellis SS, Weiss SA, et al. The ictal wavefront is the spatiotemporal source of discharges during spontaneous human seizures. Nat Commun. 2016; 29:11098. https://doi.org/10.1038/ncomms1109.

Sperling MR, Barshow S, Nei M, Asadi-Pooya AA. A reappraisal of mortality after epilepsy surgery. Neurology. 2016; 86:1938–44. https://doi.org/10.1212/WNL.0000000000002700. [PubMed: 27164679]

Spring AM, Pittman DJ, Aghakhani Y, Jirsch J, Pillay N, Bello-Espinosa LE, et al. Interrater reliability of visually evaluated high frequency oscillations. Clin Neurophysiol. 2017; 128:433–41. [PubMed: 28160749]

Ulbert I, Maglóczky Z, Eross L, Czirják S, Vajda J, Bognár L, et al. In vivo laminar electrophysiology co-registered with histology in the hippocampus of patients with temporal lobe epilepsy. Exp Neurol. 2004; 187:310–8. [PubMed: 15144857]

Waldman Z, Shimamoto S, Song I, Orosz I, Bragin A, Fried I, et al. A method for the topographical identification and quantification of high frequency oscillations in intracranial electroencephalography recordings. Clin Neurophysiol. 2018; 129(1):308–18. [PubMed: 29122445]

Wang S, Wang IZ, Bulacio JC, Mosher JC, Gonzalez-Martinez J, Alexopoulos AV, et al. Ripple classification helps to localize the seizure-onset zone in neocortical epilepsy. Epilepsia. 2013; 54:370–6. https://doi.org/10.1111/j.1528-1167.2012.03721.x. [PubMed: 23106394]

Weiss SA, Banks GP, McKhann GM Jr, Goodman RR, Emerson RG, Trevelyan AJ, et al. Ictal high frequency oscillations distinguish two types of seizure territories in humans. Brain. 2013; 136:3796–808. [PubMed: 24176977]

Weiss SA, Lemesiou A, Connors R, Banks GP, McKhann GM, Goodman RR, et al. Seizure localization using ictal phase-locked high gamma: a retrospective surgical outcome study. Neurology. 2015; 84:2320–8. [PubMed: 25972493]

Weiss SA, Orosz I, Salamon N, Moy S, Wei L, Van't Klooster MA, et al. Ripples on spikes show increased phase-amplitude coupling in mesial temporal lobe epilepsy seizure-onset zones. Epilepsia. 2016; 57:1916–30. [PubMed: 27723936]

Weiss, SA., Asadi-Pooya, AA., Vangala, S., Moy, S., Wyeth, DH., Orosz, I., et al. AR2, a novel automatic muscle artifact reduction software method for ictal EEG interpretation: validation and comparison of performance with commercially available software. Version 2. F1000Res. 2017 Jan 10. doi: https://doi.org/10.12688/f1000research.10569.2eCollection 2017

Wiebe S, Blume WT, Girvin JP, Eliasziw M. Effectiveness and efficiency of surgery for temporal lobe epilepsy study group. A randomized, controlled trial of surgery for temporal-lobe epilepsy. N Engl J Med. 2001; 345:311–8. [PubMed: 11484687]

Worrell GA, Gardner AB, Stead SM, Hu S, Goerss S, Cascino GJ, et al. High-frequency oscillations in human temporal lobe: simultaneous microwire and clinical macroelectrode recordings. Brain. 2008; 131:928–37. https://doi.org/10.1093/brain/awn006. [PubMed: 18263625]

Zelmann R, Mari F, Jacobs J, Zijlmans M, Dubeau F, Gotman J. A comparison between detectors of high frequency oscillations. Clin Neurophysiol. 2012; 123:106–16. https://doi.org/10.1016/j.clinph.2011.06.006. [PubMed: 21763191]

Zhang M, Ladas TP, Qiu C, Shivacharan RS, Gonzalez-Reyes LE, Durand DM. Propagation of epileptiform activity can be independent of synaptic transmission, gap junctions, or diffusion and is consistent with electrical field transmission. J Neurosci. 2014; 34:1409–19. [PubMed: 24453330]

Appendix A. Supplementary material

Supplementary data associated with this article can be found, in the online version, at https://doi.org/10.1016/j.clinph.2017.08.036.

HIGHLIGHTS

- Applying independent component analysis (ICA) to intracranial EEG following band-pass filtering (80–600 Hz) reduces artifact.
- Ripple detection is precise after utilizing ICA to reduce and demarcate artifact.
- Ripple rates are elevated in the seizure onset zone in recordings performed during sleep and intraoperatively.

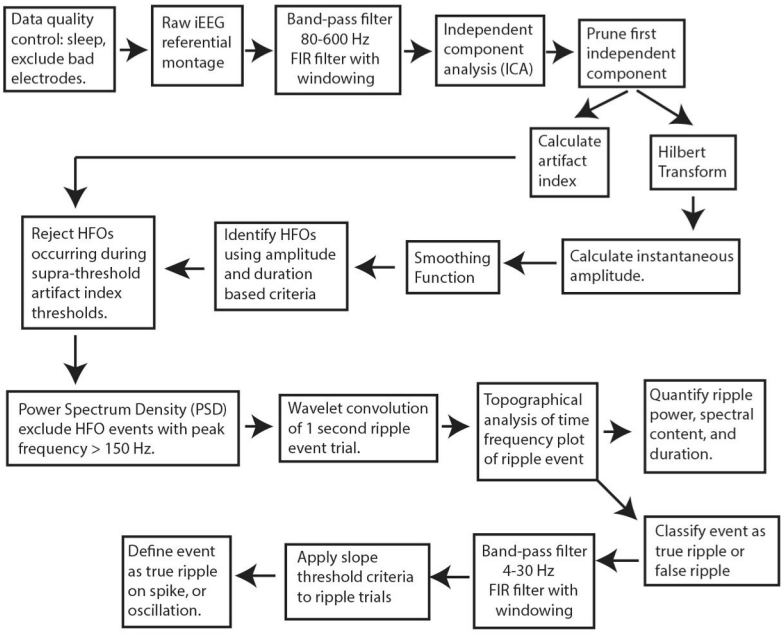

Fig. 1.

Illustration of the signal processing process for the ripple detector. Following a quality control step consisting of visual inspection to identify electrodes with poor recording quality, iEEG in referential montage is band-pass (80–600 Hz) filtered, and independent component analysis (ICA) is performed, and the resulting first independent component is pruned from the band-pass filtered signal. An artifact index is derived to demarcate artefactual HFOs. HFOs are then detected using a custom Hilbert detector and ripples are selected using power-spectral density measurements. Subsequently, a topographical algorithm is applied to the wavelet convolution of each event trial to classify each event as a true or false ripple, and quantify its properties. The true ripples are classified as events occurring on spikes or oscillations on the basis of the slope of the band-pass (4–30 Hz) iEEG during the trial.

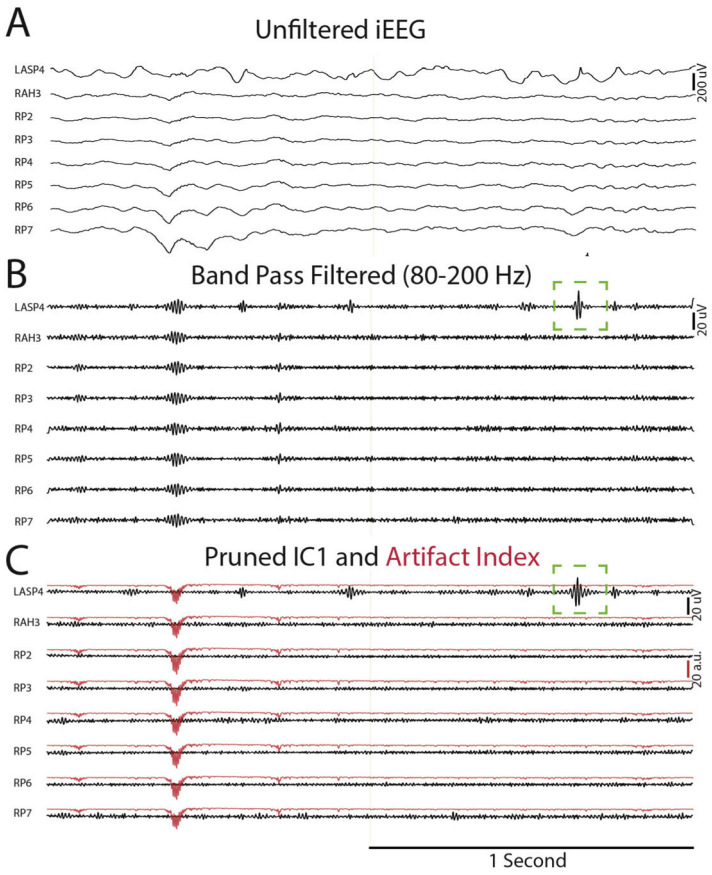

Fig. 2.

Illustration of the utilization of independent component analysis (ICA) for artifact reduction, rejection of artefactual ripples, and improvement in ripple signal to noise. An iEEG recording from eight contacts in referential montage (A) demonstrates no obvious artifact. Band-pass (80–200 Hz) filtering (B) reveals a ripple occurring synchronously in all the recordings, follow by a ripple with an unconvincing morphology in LASP4 (green box). Performing ICA on the band-pass filtered signal and pruning independent component 1 (C) results in the elimination of the first ripple in all the recordings, and the unmasking of additional oscillatory cycles in the subsequent ripple in LASP4 (green box). The artifact index (red) indicates the epoch in which the artefactual HFO contaminated the recording. (For interpretation of the references to color in this figure legend, the reader is referred to the web version of this article.)

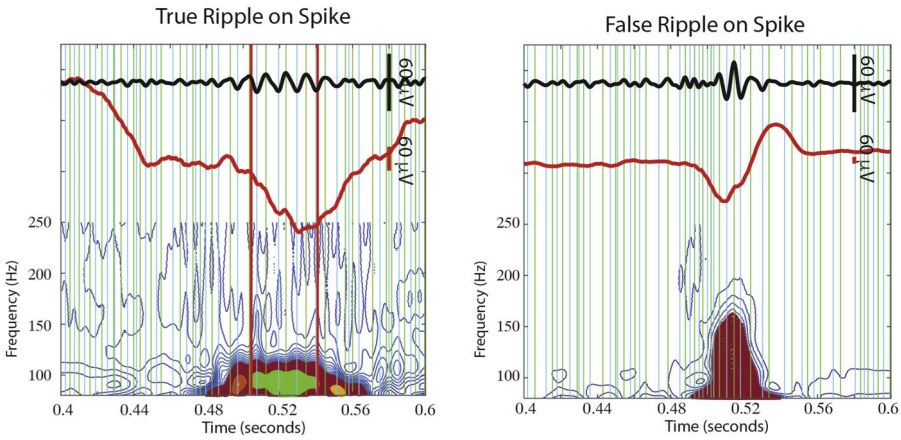

Fig. 3.

Topographical analysis of isopower contours applied to time-frequency plots of ripple event trials. The 80–240 Hz band-pass filtered iEEG waveforms, (Middle, red) unfiltered iEEG waveform, (bottom) time-frequency representation of the iEEG waveform following contour processing, and closed loop detection algorithms, with the group of closed loop contours representing the ripple shown in green, and the group of open loop contours representing the spike shown in magenta. Green and blue vertical line are positive and negative peaks in the band-pass filtered signal, respectively. Vertical red lines indicate the beginning and end times of the characterized ripple event. (For interpretation of the references to color in this figure legend, the reader is referred to the web version of this article.)

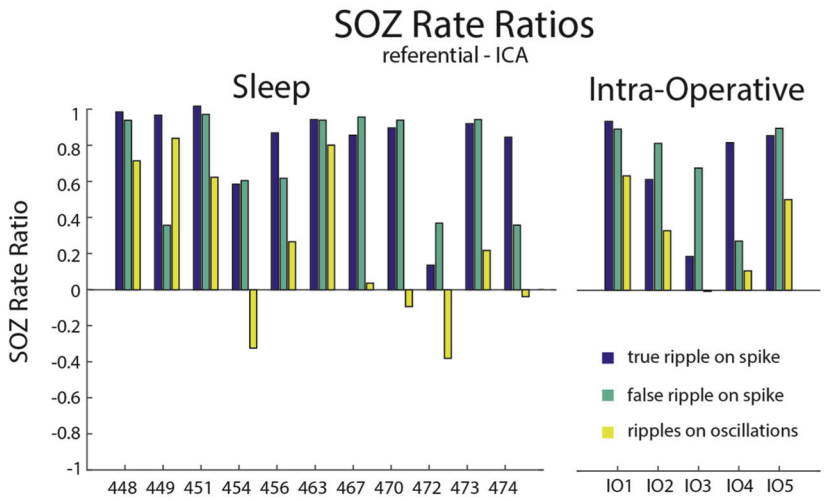

Fig. 4.

True and false ripple on spike rates defined by the detector are increased in the seizure onset zone. (A) The seizure onset zone rate ratio for true ripples on spikes (blue), false ripples on spikes (green), and ripples on oscillations (yellow) for each of the 17 patients. (For interpretation of the references to color in this figure legend, the reader is referred to the web version of this article.)

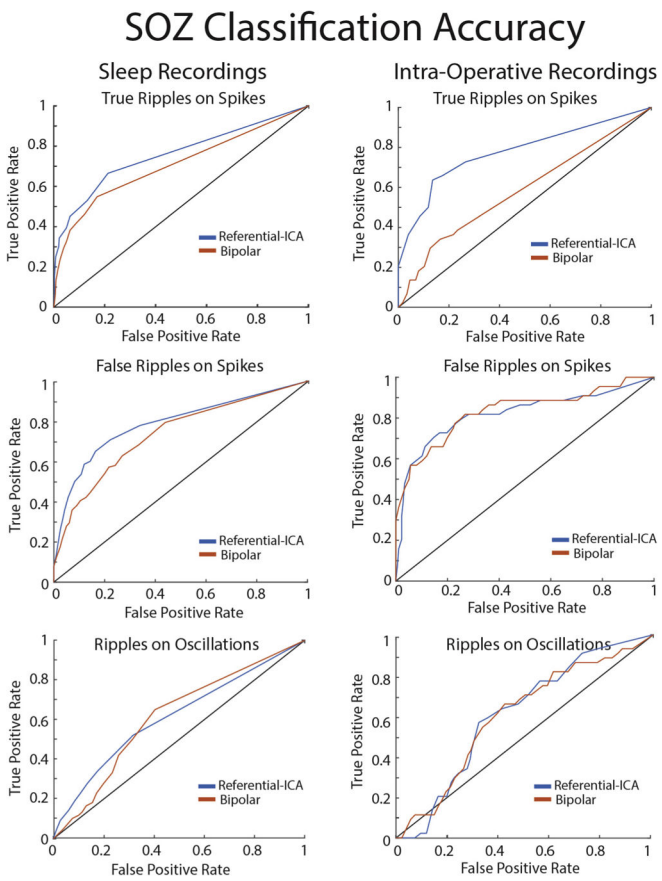

Fig. 5.

The classification accuracy of ripple rates for the seizure onset-zone (SOZ) for the different ripple types detected using referential or bipolar montage. Receiver operating characteristic curves for classifying the SOZ using the rates of true ripples on spikes (top), false ripples on spikes (middle), and ripples on oscillations (bottom) derived from recordings from sleep (left) and in the operating room (right) in referential montage (blue) or bipolar montage (red). (For interpretation of the references to color in this figure legend, the reader is referred to the web version of this article.)

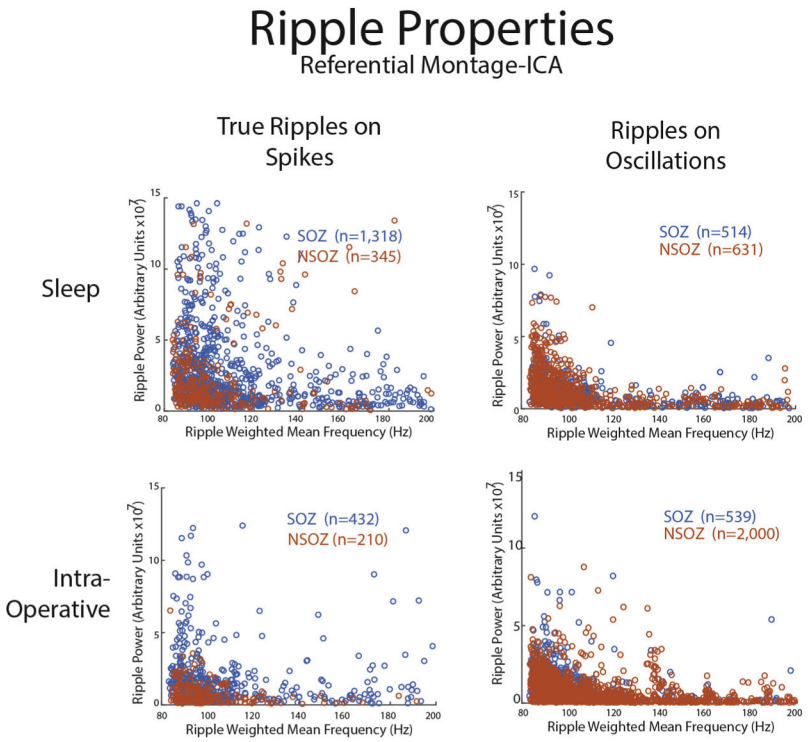

Fig. 6.

Differences in the spectral content and power of ripples inside and outside the seizure onset zone. Weighted mean frequency and power of true ripples on spikes (left) and ripples on oscillations (right) inside (blue) and outside (red) of the seizure onset zone derived from the referential recordings during sleep (top), and in the operating room (right). (For interpretation of the references to color in this figure legend, the reader is referred to the web version of this article.)

Table 1

Patient characteristics. iEEG recordings for UC, *i.e.* University of California Los Angeles, patients were performed in the EMU during mixed-stage sleep, whereas recordings for TJU, *i.e.* Thomas Jefferson University, patients were performed in the operating room. iEEG: intracranial EEG, IED: inter-ictal epileptiform discharge, SOZ: seizure-onset zone. N/A: not applicable i.e. no resection, FCD: focal cortical dysplasia.

Patient Age Sex		Epilepsy Duration	Risk Factors	Scalp EEG	MRI	PET Hypometabolic	iEEG IED	iEEG SOZ	Pathology
1.	UC_448 52 M	16 yrs	Stroke	Left temporal	Left PCA infarct	Left temporal	Left mesial and neocortical temporal	Left mesial temporal	Gliosis
2.	UC_449 36 M	24 yrs	Stroke	None	None	Left perisylvian	Left parietal-occipital	Left parietal-occipital	Gliosis
3.	UC_451 52 F	22 yrs	NF1	Left and right temporal	Right inferior gyrus T2 signal	Left temporal	Left and right mesial temporal	Left and right mesial temporal	N/A
4.	UC_454 45 M	34 yrs	Meningitis	Left temporal	T2 signal in left lateral temporal lobe	Left frontal, insular, and temporal lobe	Left frontal, insular, and temporal	Left frontal, insular, and temporal	N/A
5.	UC_456 35 F	12 yrs	None	Right temporal	Normal s/p RNS removal	Right temporal	Right mesial temporal	Right mesial and lateral temporal	Gliosis
6.	UC_463 27 M	10 yrs	None	Left and right temporal	Right hippocampal sclerosis, prior right AVM resection	Hypometabolism around prior AVM resection	Right and left mesial temporal	Right and left mesial temporal.	None
7.	UC_467 23 F	16 yrs	None	Left centro-parietal	Left parietal focal cortical dysplasia	Left parietal and occipital	Left parietal	Left parietal	FCDIIb
8.	UC_470 49 F	30 yrs	None	Left temporal	Left hippocampal sclerosis	Left temporal	Left mesial temporal	Left mesial temporal	None
9.	UC_472 43 F	27 yrs	Febrile seizures	Left and right temporal	R. temporal craniotomy and hippocampal resection	Right temporal	Left mesial temporal, right orbitofrontal	Left mesial temporal, right orbitofrontal	N/A
10.	UC_473 69 M	5 yrs	TBI	Left and right temporal	Left hippocampal sclerosis	Left temporal and orbitofrontal	Left and right mesial temporal	Left mesial temporal	None
11.	UC_474 43 F	6 yrs	TBI	Left	Microbleed in right centrum ovale	Right temporal	Left and right mesial temporal	Left and right mesial temporal	None
12.	TJU_001 51 M	13 yrs	TBI	Left and right temporal	Left temporal encephalocele	Left temporal tip	Left and right mesial temporal	Left mesial temporal	N/A

Patient Age Sex		Epilepsy Duration	Risk Factors	Scalp EEG	MRI	PET Hypometabolic	iEEG IED	iEEG SOZ	Pathology
13.	TJU_002 52 M	19 yrs	TBI	Left and right temporal	Bilateral hippocampal atrophy	Right temporal	Left and right mesial temporal	Left and right mesial temporal	N/A
14.	TJU_004 29 M	29 yrs	Premature birth	Left occipital	Normal	Left temporal and occipital	Left hippocampal, occipital, and parietal	Left occipital and parietal	N/A
15.	TJU_005 41 M	41 yrs	Febrile seizures	Right temporal	Prior right hippocampal sparing anterior temporal lobectomy	N/A	Right mesial temporal	Right mesial temporal	N/A
16.	TJU_006 33 M	13 yrs	TBI	None, seizures obscured	Normal	Normal	Right Frontal (motor)	Right Frontal (motor)	N/A

Table 2

Results of the validation of the ripple detector on the basis of visual inspection of annotated iEEG recordings. %FN = 0 refers to the percentage of eight-minute recordings from individual recording electrodes in which the detector correctly annotated each and every ripple event, or no ripple events.

Patient (n = ripple events)	Sensitivity	Precision	%FN = 0
UC_448 (n = 136)	84.61%	87.61%	50%
UC_449 (n = 265)	89.58%	91.49%	40%
UC_451 (n = 105)	90.42%	94.44%	60%
UC_454 (n = 250)	70.28%	99.43%	0%
UC_456 (n = 1115)	**53.14%**	97.00%	0%
UC_463 (n = 178)	85.06%	87.91%	60%
UC_467 (n = 816)	74.52%	96.08%	30%
UC_470 (n = 349)	90.11%	96.78%	50%
UC_472 (n = 330)	72.75%	97.91%	20%
UC_473 (n = 245)	85.65%	94.71%	40%
UC_474 (n = 79)	85.50%	90.77%	40%
TJU_001 (n = 172)	71.25%	92.68%	30%
TJU_002 (n = 812)	70.00%	96.68%	0%
TJU_004 (n = 783)	95.50%	84.80%	30%
TJU_005 (n = 165)	87.96%	63.00%	20%
TJU_006 (n = 42)	64.00%	89.00%	50%

Bold and underling signify recordings with “HFO stripping”.